Self-organized TiO_2 Nanotubes Grown on Ti Substrates with Different Crystallographic Preferential Orientations: Local Structure of TiO_2 Nanotubes vs. Photo-electrochemical Response

Miloš Krbal[a], Hanna Sopha[a], Darius Pohl[b], Ludvik Benes[c], Christine Damm[b], Bernd Rellinghaus[b], Jaroslav Kupčík[d], Petr Bezdička[d], Jan Šubrt[d], Jan M. Macak[a,e*]

[a]*Center of Materials and Nanotechnologies, Faculty of Chemical Technology, University of Pardubice, Nam. Cs. Legii 565, 53002 Pardubice, Czech Republic*

[b] *Department of Metastable and Nanostructured Materials, Institute for Metallic Materials, Leibniz-Institute for Solid State and Materials Research IFW Dresden, Helmholtzstr. 20, 01069 Dresden, Germany*

[c] *Joint laboratory of Solid-State Chemistry, Faculty of Chemical Technology, University of Pardubice, Studentska 95, 532 10 Pardubice, Czech Republic*

[d]*Institute of Inorganic Chemistry of the CAS, v.v.i., č. p. 1001, 250 68 Husinec-Řež, Czech Republic*

e Central European Institute of Technology, Brno University of Technology, Purkynova 123, 61200 Brno, Czech Republic

**Corresponding Author: e-mail: jan.macak@upce.cz,* [1] ISE Member

Phone: +420-466 037 401

Abstract

Here we report on structural properties and the photo-electrochemical response of annealed TiO_2 nanotube layers, grown on four different Ti substrates by an identical anodization process. TiO_2 nanotube layers were grown on Ti substrates by anodization in glycerol containing NH_4F and water. The layers were then annealed at 400 °C for 1 hour in air. Photocurrent densities of annealed nanotubes were recorded upon irradiation with ultraviolet (UV) light at a constant potential of 0.4 V, in a 0.1 M Na_2SO_4 aqueous solution. Approximately, a 280 % difference in the photocurrent densities was recorded from TiO_2 nanotubes fabricated from different Ti substrates. To elucidate the origin of this difference, the nanotube layers were scrutinized by Mott-Schottky measurements, X-ray diffraction (XRD) and Electron Energy Loss Spectroscopy (EELS). Inspection of the XRD patterns revealed preferential crystallographic orientations in various Ti substrates from which TiO_2 nanotube layers were produced. Subsequent EELS analyses of the annealed nanotube layers disclosed significant differences in the Ti:O stoichiometry, in accordance with XRD evaluation of preferential orientation differences among used Ti substrates.

Keywords: TiO_2 nanotubes, Anodization, Anatase, Photo-current, Stoichiometry

1. Introduction

Titanium dioxide (TiO_2) is one of the most promising semiconductors for photo-electrochemical applications, particularly due to its non-toxicity, low cost and stability against photo-corrosion. Self-organized TiO_2 nanotubes represent a very promising architecture for the fabrication of highly efficient TiO_2 electrodes. This is because the nanotubes not only present a large surface area for enhanced light absorption in their one-dimensional ordered structure, but their straight walls might also offer a direct path for photo-generated electrons towards the underlying Ti metal back contact. Stimulated by initial reports of Assefpour-Dezfuly et al. in 1984 [1] and of Zwilling et al. in 1999 [2], the formation of TiO_2 nanotubes by anodization of Ti has gained a lot of attention within past 12 years, owing to their wide range of applications [3-7]. Since then, parameters influencing the nanotube growth and dimensions, such as different electrolytes [8-11], anodization potential and time [12-14], and the electrolyte aging process were studied in great detail [15]. Comprehensive reviews are available that summarize these important aspects [16-18]. Until now, the majority of reports published on the applications of TiO_2 nanotubes is related to their photo-electrochemical properties, utilized in photo-catalysis [19], dye-sensitized solar cells [20], and water splitting [21].

Different studies have been carried out to understand the relationship between the photo-electrochemical performance of the nanotube layers and (i) nanotube dimensions [22-24], (ii) the annealing process [25-27], (iii) doping [24, 28-30], (iv) water content in the electrolyte [31,32], and (v) alteration of the tube geometry [33-35]. For example, Liu et al. [26] has shown that between different annealing processes, such as thermal annealing, water annealing and hydrothermal annealing, the thermal annealing process is the most favourable approach for optimum performance of the nanotubes in applications utilizing the UV as well as the VIS light illumination. On the other hand, Schmuki et al. [24, 29] and Regonini et al. [30] utilized Nb doping of the TiO_2 nanotubes to further improve photo-electrochemical response of their nanotube layers. However, no study until now has been conducted that would investigate the photo-electrochemical response of self-organized TiO_2 nanotubes grown on different Ti substrates obtained from different suppliers with different purity and texture. It can be expected that the structural and compositional variations in the different Ti substrates will be reflected in the structural as well as photo-electrochemical response of the TiO_2 nanotube layers grown from them. Recently, we reported on different nanotube dimensions and ordering of the nanotube layers grown on different Ti substrates used for anodization [36], taking into account the roughness of different substrates, the microstructure

and different impurities of the Ti thin foils (revealed by GD-OES). Especially, these metallic impurities could be potentially embedded in various forms in the TiO_2 nanotube layer grown by anodization and thus they could influence subsequent properties of these nanotube layers. In the literature, however, no clear answer or at least relevant discussion on the metallic impurities and their influence on the nanotube growth has been provided until now, potentially also due to a limited number of techniques able to reveal extremely small differences in the stoichiometry of TiO_2 nanotubes.

In order to address this point, we prepared anodic TiO_2 nanotube layers on different Ti substrates under as identical conditions as possible to yield nanotube layers with as similar dimensions as possible. In the next step, we carried out photo-electrochemical analyses of TiO_2 nanotube layers under ultraviolet (UV) light illumination. To elucidate the differences in the photo-electrochemical performance, we analysed structural differences in the TiO_2 nanotube layers by a range of techniques: Energy-dispersive X-ray spectroscopy (EDX), Transmission Electron Microscopy (TEM), X-ray diffraction (XRD) and Energy electron loss spectroscopy (EELS).

2. Experimental

Four types of Ti substrates (foils) of different purity, commonly used for the TiO_2 nanotube growth by researchers worldwide, were purchased from three established suppliers for comparison; Sigma-Aldrich (0.127 mm, 99.7 % purity, marked as SiAl), Advent Materials (0.125 mm, 99.6+% purity, marked as AM), Goodfellow (0.125 mm, 99.6+% purity, marked as GoFe99.6) and Goodfellow (0.125 mm, 99.99% purity, marked as GoFe99.99). Detailed information about impurities and surface roughness of used Ti substrates can be found in the work [36].

Prior to anodization the Ti substrates were degreased by sonication in isopropanol and acetone. Subsequently, the substrates were rinsed in isopropanol and dried in air. A two-electrode setup was employed for anodization, consisting of a Pt sheet as the counter electrode and the Ti substrate, pressed against an O-ring of the electrochemical cell leaving exactly 1 cm^2 open to the electrolyte, as working electrode. The electrochemical experiments were carried out at room temperature using a high-voltage potentiostat (PGU-200V, IPS Elektroniklabor GmbH). A glycerol based electrolyte containing 0.27 M NH_4F and 50 vol.% H_2O was used for anodization of Ti foils at 20 V (achieved with a sweep rate of 1 V/s) for 100 min. The temperature of the bath was kept at constant value of 22°C without stirring of the electrolyte during anodizations. In the final step, the anodized samples were sonicated in

isopropanol and dried in air. In order to convert amorphous nanotubes to nanotubes with a defined anatase structure, all samples were annealed in a muffle oven at 400 °C for 1 h in air with a heating and cooling rate of 2 °C/min. These annealing conditions were chosen based on our previous optimization [37]. We have produced 2 sets of TiO_2 nanotube layers from each type of Ti sheets to verify the reproducibility of both their structures and properties.

The structure and morphology of the TiO_2 nanotube layers was characterized by a field-emission electron microscope (FE-SEM JEOL JSM 7500F). Dimensions of the nanotubes were measured and statistically evaluated using proprietary Nanomeasure software. For each condition used in this work, we calculated average values and standard deviations from at least 3 different locations on 2 samples of each condition, with a high number of measurements ($n \geq 100$).

Chemical composition of the TiO_2 nanotube layers was analysed using an EDX system (Inca, Oxford Instruments) equipped with silicon crystal X-ray detector suitable for detection of light elements from carbon, embedded within a high resolution TEM (HR-TEM) microscope JEM 3010 (JEOL Ltd., a thermo-emission LaB_6 cathode, operated at 300 kV).

All photocurrent measurements were carried out in an aqueous electrolyte containing 0.1 M Na_2SO_4 at a constant potential of 0.4 V vs 3M Ag/AgCl, employing a photoelectric spectrophotometer (Instytut Fotonowy) connected with the modular electrochemical system AUTOLAB (model "PGSTAT 204", Metrohm Autolab B.V.) operated with *Nova 1.10* software. A three-electrode cell with a flat quartz window was employed with a Ag/AgCl reference electrode, a Pt wire counter electrode and the anodized and annealed Ti substrate as working electrode, pressed against an O-ring of the electrochemical cell leading to an irradiated sample area of 0.28 cm^2. The wavelength dependence of photocurrent densities was measured using a monochromatic light source provided with a 150 W Xe lamp and a universal grating monochromator, with a bandwidth of 5 nm. Monochromatic light employed for excitation was chopped with a shutter between light and dark phases with the interval of 10 s. Further to that, the photocurrent density transients were measured at a constant wavelength of 340 nm (which is the wavelength showing maximum photocurrent) with a light intensity of 1.8 $\mu W/cm^2$. For this particular experiment, the monochromator shutter was opened for 1000 s to obtain a stable plateau of the photocurrent values. Cyclic voltammograms were recorded in the range of potentials from -0.4 V to 1 V vs. 3 M Ag/AgCl with a sweep rate of 5 mV/s, started at 0 V towards positive voltages in the dark and under UV exposure (340 nm), respectively. Mott–Schottky plots were collected at an AC frequency of 1.0 kHz in the dark.

The crystallinity of TiO_2 nanotube layers was measured using the D8 Advance Bruker X-ray diffractometer set to Cu-K line. Structural and local chemical characterization was conducted on an aberration-corrected high resolution transmission electron microscopy (FEI Titan^3 80-300) operated at 300 kV (equipped with a field emission gun, CEOS CetCor image C_S-corrector, FEI DCOR probe C_S-corrector, high angle annular dark field (HAADF) detector and GatanTridiem 863ER for electron energy loss spectroscopy (EELS). The convergence semi-angle of the probe forming system was set to 30 mrad. The EEL spectra are measured with a collection semi-angle of the spectrometer of 28 mrad.

3. Results and discussion

For the purpose of comparison of the TiO_2 nanotube layers (grown on different substrates) by means of photo-electrochemical experiments, it was necessary to employ highly uniform and crack-free nanotube layers. Fig. 1a shows an example of a very uniform, crystalline TiO_2 nanotube layer grown on the GoFe99.99 substrates after anodization, in the cross-sectional view. Fig. 1b provides an overview of dimensions of the TiO_2 nanotube layers grown on all utilized Ti substrates. Although identical anodization conditions were employed for all 4 substrates, the average nanotube layer thickness varied between ~1.09 μm for SiAl, ~1.14 μm for AM, ~1.15 for GoFe99.6 and ~1.18 μm for GoFe99.99 substrate while the nanotube diameter was nearly the same ~78±1 nm. The origin for these variations was already discussed in detail in our recent work [36]. Briefly, differences in the nanotube dimensions were shown to be caused by the different roughness, microstructure, and the purity of the Ti substrates. However, the means of thickness and diameter values of all tube layers were within standard deviation values of all tube layers (represented by error bars in Fig. 1B). No significant differences were observed in the shape and thickness of the tube walls among the different nanotube layers. All tubes had regular ripples on their walls, which is a very typical feature for the anodic TiO_2 nanotubes [16-18].

All nanotube layers were investigated very thoroughly by EDX mapping and a through a high-resolution TEM analyses and no metal-based impurities within nanotubes (that would stem from impurities of substrates) were found.

Fig. 2A, B shows the photocurrent densities and the incidence of photon conversion efficiency (IPCE) recorded in the range of wavelengths from 300 to 400 nm with a step of 5 nm for the TiO_2 nanotube layers grown on all different substrates. Fig. 2 C and D show in detail transients of photocurrent densities recorded during the ON/OFF photocurrent measurement as well as upon long illumination (at λ = 340 nm, light was ON for 1000 s),

respectively. Ideally, TiO_2 nanotube layers grown under the same conditions should express similar photocurrent densities. However, significant differences among the obtained photocurrent densities were observed. One can see from Fig. 2 that photocurrent density at λ = 340 nm increases from 39.5 μA/cm^2 for SiAl, 45 μA/cm^2 for GoFe99.6, 68 μA/cm^2 for AM to 112 μA/cm^2 for GoFe99.99 which is ~ 280 % difference between the best and the worst values. Interestingly, IPCE for GoFe99.99 reaches nearly 100% in the measured UV spectral region (300-330 nm). Since nanotube dimensions are very similar, it can be assumed that essentially the same portion of the UV light photons is absorbed within the nanotube layers resulting in the charge carrier generation [28]. Thus, the photocurrent should be governed by the number of electrons arriving at the collecting electrode, in this case at the Ti substrates. Therefore, the main reasons for the photocurrent variations seem to be related to the character and number of recombination sites - traps in the nanotube layers. Obviously, the saturation of these unwanted traps requires some time - on the scale from seconds (GoFe99.99 and AM) to minutes (SiAl and GoFe99.6). Therefore, in general after approximately 150 seconds of continuous irradiation, the photocurrent densities shown in Fig. 2D become stable.

To further provide a deeper electrochemical understanding of all nanotube layers cyclic voltammograms were recorded in the range of -0.4 V and +1 $V_{vs.\ Ag/AgCl}$. Fig. 3A displays CV curves obtained in the dark (solid lines) and under the UV light illumination (λ = 340 nm, dashed lines), respectively. It was found that the dark currents were nearly identical for all TiO_2 nanotube layers, whereas the photocurrent densities increased until a potential of ≈ 0.4 V. For potentials higher than 0.4 V a photocurrent saturation was observed which indicated that the nanotube wall thickness became equal to the space charge layer [22]. It should be pointed that except of the maximum values of photocurrent densities the electrochemical behaviour of all studied samples upon UV light exposure was similar.

Additionally, we explored electronic properties of all prepared TiO_2 nanotube layers by means of the Mott-Schottky theory [27] to obtain information about the flatband potential - U_{fb} and majority carrier densities - N_D. Under assumption that the Helmholtz layer can be omitted, data can be plotted following Eq. (1):

$$\frac{1}{C^2} = \frac{2}{\varepsilon\varepsilon_0 q N_D A^2}\left(U - U_{fb} - \frac{kT}{q}\right)$$

where C is the space charge capacitance, ε dielectric constant, ε_0 the vacuum permittivity, q the charge of the electron, N_D the donor concentration, A the area, U the

applied potential, U_{fb} the flatband potential and the expression –kT/q is equal to 25 mV at room temperature.

Figure 3B exhibits the Mott-Schottky plots for TiO_2 nanotube layers grown on different Ti substrates. The slope of all Mott-Schottky curves is positive which is characteristic for n-type semiconductors. The U_{fb} can be determined by extrapolation of linear part $1/C^2$ to 0. From Fig. 3B one can see that the value of the U_{fb} for the GoFe99.99 is ≈ 0.02 V whereas U_{fb} for the other samples reaches ≈ 0.18 V vs. Ag/AgCl. The more negative U_{fb} value of the GoFe 99.99 sample indicates a shift of the conduction band to more positive potentials [38]. We also evaluated from the Mott-Schottky plots majority carrier densities (N_D) to assess the level of oxygen vacancies (that are typically considered as major defects in the TiO_2 lattice) and other defects in general. The N_D values were $3.8x10^{18}$, $6.1x10^{18}$, $6.3x10^{18}$ and $7.8x10^{18}$ cm^{-3} for GoFe99.6, AM, GoFe 99.99 and SiAl substrates, respectively. The trends in photocurrent densities follow trends in N_D, except the SiAl sample, which has the lowest photocurrent and the highest N_D. This means that the differences in photocurrents among all samples cannot be explained straight away by differences in their N_D values.

To obtain a deeper insight about the photocurrent differences, it is necessary to consider also the space charge region and the bend bending of the various nanotube layers. It can be seen that AM and GoFe99.99 layers possess a similar slope of the linear region of the Mott-Schottky plots. However, the GoFe99.99 has more pronounced band bending, derived from the more cathodic flat band potential, which is translated into wider space charge region. This yields the highest photocurrent for GoFe99.99 sample and the second highest photocurrent for AM samples. On the other hand, SiAl has the lowest slope and considering its U_{fb} it has comparably smaller space charge region than other samples. This yields the lowest photocurrent for SiAl samples. The remaining sample – GoFe99.6 – is in between with the photocurrent yield, even though it possesses a comparably wider space charge region at a constant bend bending than other samples. This wider region, however, itself cannot justify substantially higher photocurrents. This sample possesses also the highest slope from the Mott-Schottky plots (i.e. it is the most insulating in terms of N_D). Thus the average electric field in the GoFe99.6 sample is lower than in other samples, and as a matter of fact a larger amount of photogenerated carriers recombines under this lower electric field.

In addition, the more negative U_{fb} for the GoFe99.99 is a sign of better electronic conductivity of nanotubes, as recently reported on Ti^{3+} self-doped TiO_2 nanotube layers [39, 40]. However, one has to take in account also that the difference in the observed U_{fb} can also

particularly stem to the distinct surface chemistry of TiO_2 nanotube walls since the value of U_{fb} strongly depends on the concentration of surface hydroxyl groups [41].

In order to gain more insight into this fundamentally interesting issue, XRD and EELS investigations were performed to reveal further differences among the tube layers. Fig. 4 shows XRD patterns recorded under the same conditions for all four nanotube layers annealed at 400 °C for 1 hour. All TiO_2 nanotube layers crystallize in the anatase modification belonging to the space group $I4_1/amd$ [42] with the most intensive peak at $2\theta \approx 25.4^o$ which corresponds to the <101> diffraction line. Upon a detailed analysis of the peak position, no shift in position between the different nanotube layers from the nominal value was observed. Titanium substrates can be found in the $P6_3/mmc$ space group [43]. Strikingly, one can see from Fig. 4 that GoFe99.99 and AM metallic titanium sheets possessed preferential orientations while XRD spectra for GoFe99.6 and SiAl substrates were mainly identical. The maximum peak intensity for GoFe99.99 was located at $2\theta \approx 63.1^o$ and AM peaks at $2\theta \approx 70.6^o$ which corresponds to the <110> and <103> diffraction lines, respectively. The maximum intensity of XRD patterns for GoFe99.6 and SiAl substrates was found at $2\theta \approx 38.5^o$ which was assigned to the <002> diffraction line of Ti.

These results evoke one to suppose that anodic growth of TiO_2 nanotube layers from differently oriented Ti metallic substrates could generate various numbers of electron traps as well as Ti ions in different oxidation states which might significantly influence the charge transport. Hence, to study the Ti:O stoichiometry in all TiO_2 nanotube layers, we collected EELS spectra from the Ti $L_{2,3}$ edge which are shown in Fig. 5. A cross-sectional scanning-TEM image of a typical area of EELS data acquisition of TiO_2 nanotube layers is depicted in Fig.4 A. Fig. 4 B and C demonstrate Ti $L_{2,3}$ edge with characteristic spin–orbit splitting into $2p_{3/2}$ (L_3) and $2p_{1/2}$ (L_2) levels and the peak separation of 5.4 eV [44]. Further band splitting of Ti 3d states into the t_{2g} ($3d_\pi$) and e_g ($3d_\sigma$) symmetries corresponds to the octahedrally coordinated Ti atoms with O atoms [44]. Similarly, the peak splitting observed in O K edge (Fig. 4D) is attributed to O 2p-Ti 3d hybridized states of t_{2g} and e_g symmetry. EELS spectra of metallic Ti substrates (Fig. 5B) appear very similar, however, detailed analyses of normalized spectra disclosed that the band corresponding to Ti L_3 edge for the GoFe99.99 sample has a lower intensity in parallel with GoFe 99.6 and SiAl substrates. The same holds true for the AM substrate in a lesser extent. Since there is no evidence of the oxygen atoms at 530 eV one may assume that this difference is related to the preferential orientation observed in used metallic Ti substrates. In contrast, all TiO_2 nanotube layers were found to be in the same crystallographic orientation (see Fig 4.) which implies that the aspect of the different

preferential orientation does not have to be considered for the further evaluation of the Ti $L_{2,3}$ edge EELS spectra. In the view of the shape of EELS spectra in Fig. 4C, SiAl curve shows the most pronounced t_{2g} and e_g splitting, which nearly perfectly corresponds to the anatase modification. It is followed by the GoFe99.66 curve with a bit smeared out spectrum. It is followed by the AM curve with even less evolved splitting. Finally the spectrum of the GoFe99.99 sample consists of broad L_2 and L_3 bands. The latter spectrum resembles well the recently published spectrum of amorphous TiO_2 [45]. However, amorphous TiO_2 does not generate strong photocurrent and also the XRD pattern revealed that the studied nanotube layer of GoFe99.99 is well crystalline. Thus the origin of the broad peak should be a sign of distinct Ti:O ratio in the nanotube layer. As it is evident from the investigation of Ti $L_{2,3}$ edge EELS spectra of Ti_xO_y [46], peaks become broader and their maxima are shifted to the lower loss energy from TiO_2 (anatase) to TiO (cubic) structures. Based on these reported results, the Ti $L_{2,3}$ edge EELS of GoFe99.99 could be assigned to the Ti_3O_5 compound, AM is similar to the Ti_4O_7 structure, GoFe99.6 resembles the Ti_5O_9 structure and SiAl is nearly close to the TiO_2 anatase phase. Significant oxygen deficiency of the nonstochiometric TiO_2 nanotube layer grown on GoFe99.99 is corroborated by O K edge where characteristic t_{2g} (530 eV) and e_g (533 eV) splitting existing in the anatase modification is merged in one band with its maximum peaking at 532.5 eV which is in line with recently published data [47].
Therefore, while from the crystallographic point of view, the nanotube layers grown on different substrates seem to be similar, the EELS data showed that TiO_2 nanotube layers grown on GoFe99.99 were the most oxygen deficient. Since dimensions for all nanotube layers were basically the same (within the standard deviation represented by error bars in Fig. 1B) and material properties were in general linked to the structure (including defects), one can induce that the greatest photocurrent observed for GoFe99.99 results from the highest concentration of Ti^{3+} or oxygen vacancies, which is in line with the recent report on reduced TiO_2 nanotube layers [40].

However, as derived from the photocurrent measurements, the N_D for GoFe99.99 is lower than for the SiAl sample with the lowest photocurrent. In fact, this clearly shows that the differences among the nanotube layers are of more complex nature and involve an interplay between the oxygen vacancies, presence of Ti^{3+} interstitials within TiO_2 nanotubes, widths of the space charge regions, the electronic conductivity of the nanotubes, grain boundaries and also the presence of other dopants. It can be expected, based on impurities present in substrates (such as Fe,V or Al, according to GDOES, as shown in Ref. 36) that there are likely some dopants present in a certain amount within nanotubes based on these

impurities. However, their amount is so low that it is not traceable by EDX or XPS or any other reasonably accessible or available surface analytical tool and therefore it cannot be properly quantified.

All in all, from the presented results it is clear that the choice of the Ti substrate for the tube growth has an impact on the UV light driven photo-electrochemical response of the tubes grown on the substrates. More efforts have to be carried out to understand the role of preferential crystallographic orientation in Ti substrates on the growth of TiO_2 nanotube layers and resulting Ti:O stoichiometry, which have implication on the conversion of the amorphous tube walls into the anatase structure when annealed.

4. Conclusions

In conclusion, self-organized TiO_2 nanotube layers grown on different Ti substrates from different suppliers showed large variations in the photo-electrochemical response upon UV illumination (approximately 280 % difference between lowest and highest photocurrent densities). Investigations by XRD showed that Ti substrates differ from each other in preferential crystallographic orientations and also that the originally amorphous nanotubes were converted into crystalline anatase nanotubes. Further, detailed EELS analyses revealed significant differences in the Ti:O stoichiometry and that all TiO_2 nanotubes were oxygen deficient. It was found that the highest photocurrent density generate TiO_2 nanotube layers with the highest content of Ti^{3+} ions. These results clearly demonstrate that for an efficient utilization of the TiO_2 nanotube layers, a proper selection of the Ti substrate might be very important to carry out subsequent photo-electrochemical studies on the nanotube layers.

Acknowledgments

European Research Council (project nr. 638857) and Ministry of Youth, Education and Sports of the Czech Republic (projects nr. LM2015082, CZ.02.1.01/0.0/0.0/16_013/0001829, LQ1601) are acknowledged for financial support of this work. Authors thank Dr. Veronika Podzemna for SEM analyses.

References

[1] M. Assefpour-Dezfuly, C. Vlachos, E. H. Andrews, Oxide morphology and adhesive bonding on titanium surfaces, J. Mater. Sci. 19 (1984) 3626.

[2] V. Zwilling, M. Aucouturier, E. Darque-Ceretti, Anodic oxidation of titanium and TA6V alloy in chromic media. An electrochemical approach, Electrochim. Acta 45 (1999) 921.

[3] J.M. Macak, H. Tsuchiya, A. Ghicov, P. Schmuki, Dye-sensitized anodic TiO_2 nanotubes, Electrochem. Commun. 7 (2005) 1133.

[4] O.K. Varghese, D. Gong, M. Paulose, K.G. Ong, C.A. Grimes, Hydrogen sensing using titania nanotubes, Sens. Actuators, B 93 (2003) 338.

[5] K. Gulati, S. Ramakrishnan, M.S. Aw, G. J. Atkins, D.M. Findlay, D. Losic, Biocompatible polymer coating of titania nanotube arrays for improved drug elution and osteoblast adhesion, Acta Biomater. 8 (2012) 449.

[6] J.M. Macak, M. Zlamal, J. Krysa, P. Schmuki, Self-organized TiO_2 nanotube layers as highly efficient photocatalysts, Small 3 (2007) 300.

[7] J.E. Yoo, K. Lee, A. Tighineanu, P. Schmuki, Highly ordered TiO_2 nanotube-stumps with memristive response, Electrochem. Commun. 34 (2013) 177.

[8] R. Beranek, H. Hildebrand, P. Schmuki, Self-organized porous titanium oxide prepared in H_2SO_4/HF electrolytes, Electrochem. Solid-State Lett. 6 (2003) B12.

[9] J.M. Macak, H. Tsuchiya, L. Taveira, S. Aldabergerova, P. Schmuki, Smooth anodic TiO2 nanotubes, Angew. Chem. Int. Ed. 44 (2005) 7463.

[10] J. M. Macak, H. Tsuchiya, L. Taveira, S. Aldabergerova, P. Schmuki, Smooth Anodic TiO2 Nanotubes, Angew. Chem. Int. Ed. 44 (2005) 7463.

[11] S.P. Albu, A. Ghicov, J.M. Macak, P. Schmuki, 250 μm long anodic TiO_2 nanotubes with hexagonal self-ordering, Phys. Stat. Sol. (RRL) 1 (2007) R65.

[12] J.M. Macak, H. Tsuchiya, A. Ghicov, K. Yasuda, R. Hahn, S. Bauer, P. Schmuki, TiO_2 nanotubes: Self-organized electrochemical formation, properties and applications, Curr. Opin. Solid State Mater. Sci. 11 (2007) 3.

[13] K. Kant, D. Losic, Self-ordering electrochemical synthesis of TiO_2 nanotube arrays: Controlling the nanotube geometry and the growth rate, Int. J. Nanosci. 10 (2011) 55.

[14] L. Yin, S. Ji, G. Liu, G. Xu, C. Ye, Understanding the growth behavior of titania nanotubes, Electrochem. Commun. 13 (2011) 454.

[15] H. Sopha, L. Hromadko, K. Nechvilova, J.M. Macak, Effect of electrolyte age and potential changes on the morphology of TiO_2 nanotubes, J. Electroanal. Chem., 759 (2015) 122.

[16] J. M. Macak, H. Hildebrand, U. Marten-Jahns, P. Schmuki, Mechanistic aspects and growth of large diameter self-organized TiO_2 nanotubes, J. Electroanal. Chem. 621 (2008) 254.

[17] D. Kowalski, D. Kim, P. Schmuki, TiO_2 nanotubes, nanochannels and mesosponge: Self-organized formation and applications, Nano today 8 (2013) 235.

[18] K. Lee, A. Mazare, P. Schmuki, One-dimensional titanium dioxide nanomaterials: Nanotubes, Chem. Rev. 114 (2014) 9385.

[19] I. Paramasivam, H. Jha, N. Liu, P. Schmuki, A Review of Photocatalysis using Self-organized TiO_2 Nanotubes and Other Ordered Oxide Nanostructures, Small 8 (2012) 3073.

[20] P. Roy, D. Kim, K. Lee, E. Spiecker, P. Schmuki, TiO_2 nanotubes and their application in dye-sensitized solar cells, Nanoscale 2 (2010) 45.

[21] Z. Zhang, M.F. Hossain, T. Takahashi, Photoelectrochemical water splitting on highly smooth and ordered TiO_2 nanotube arrays for hydrogen production, Int. J. Hydrog. En. 35 (2010) 8528.

[22] R. Beranek, H. Tsuchiya, T. Sugishima, J.M. Macak, L. Taveira, S. Fujimoto, H. Kisch, P. Schmuki, Enhancement and limits of the photoelectrochemical response from anodic TiO_2 nanotubes, App. Phys. Lett. 87 (2005) 243114.

[23] R. Beranek, J.M. Macak, M. Gärtner, K. Meyer, P. Schmuki, Enhanced visible light photocurrent generation at surface-modified TiO_2 nanotubes. Electrochim. Acta 54 (2009) 2640.

[24] S. Ozkan, A. Mazare, P. Schmuki, Extracting the limiting factors in photocurrent measurements on TiO_2 nanotubes and enhancing the photoelectrochemical properties by Nb doping, Electrochim. Acta 176 (2015) 819.

[25] A. Ghicov, H. Tsuchiya, J.M. Macak, P. Schmuki, Annealing effects on the photoresponse of TiO_2 nanotubes, Phys.Stat. Sol. A 203 (2006) R28.

[26] N. Liu, S. P. Albu, K. Lee, S. So, P. Schmuki, Water annealing and other low temperature treatments of anodic TiO2 nanotubes: a comparison of properties and

efficiencies in dye sensitized solar cells for water splitting, Electrochim. Acta 82 (2012) 98.

[27] H. Tsuchiya, J.M. Macak, A. Ghicov, A.S. Räder, L. Taveira, P. Schmuki, Characterization of electronic properties of TiO_2 nanotube films, Corros. Sci. 49 (2007) 203.

[28] J. M. Macak, A. Ghicov, R. Hahn, H. Tsuchiya, P. Schmuki, Photoelectrochemical properties of N-doped self-organized titania nanotube layers with different thicknesses, J. Mater. Res. 21 (2006) 2824.

[29] M. Yang, H. Jha, N. Liu, P. Schmuki, Increased photocurrent response in Nb-doped TiO_2 nanotubes, Journal of Materials Chemistry 21 (2011) 15205.

[30] D. Regonini, A. Schmidt, C.G. Aneziris, T. Graule, F.J. Clemens, Impact of the Anodizing Potential on the Electron Transport Properties of Nb-doped TiO_2 Nanotubes, Electrochim. Acta 169 (2015) 210.

[31] L.-K. Tsui, T. Homma, G. Zangari, Photocurrent Conversion in Anodized TiO_2 Nanotube Arrays: Effect of the Water Content in Anodizing Solutions, The Journal of Physical Chemistry C 117 (2013) 6979.

[32] D. Regonini, A. A. Groff, G.D. Sorarù, F.J. Clemens, Photoelectrochemical study of anodized TiO_2 Nanotubes prepared using low and high H_2O contents, Electrochim. Acta, 186 (2015) 101.

[33] Y. Rambabu, M. Jaiswal, S.C. Roy, Enhanced photoelectrochemical performance of multi-leg TiO_2 nanotubes through efficient light harvesting, J. Phys. D: Appl. Phys. 45 (2015) 295302.

[34] S. K. Mohapatra, M. Mistra, V.K. Mahajan, K.S. Raja, Synthesis of Y-branched TiO_2 nanotubes, Mater. Lett. 62 (2008) 1772.

[35] L. Ashari, D.J.Leclere, G. Kawamura, H. Muto, A. Matsuda, Study of branched TiO_2 nanotubes and their application to dye sensitized solar cells, J. Ceram. Soc. Japan, 122 (2014) 866.

[36] H. Sopha, P. Knotek, A. Jäger, J. M. Macak, Self-organized anodic TiO_2 nanotube layers: Influence of the Ti substrate on nanotube growth and dimensions, Electrochim. Acta, 190 (2016) 744.

[37] S. Das, R. Zazpe, J. Prikryl, P. Knotek, M. Krbal, H. Sopha, V. Podzemna and J. M. Macak, Influence of annealing temperatures on the properties of low aspect-ratio TiO_2 nanotube layers, Electrochim. Acta, 213 (2016) 452.

[38] A. I. Kontos, V. Likodimos, T. Stergiopoulos, D. S. Tsoukleris, P. Falaras, Self-organized anodic TiO_2 nanotube arrays functionalized by iron oxide nanoparticles. Chem Mater 21 (2009) 662.

[39] J. Song, M. Zheng, X. Yuan, Q. Li, F. Wang, L. Ma, Y. You, S. Liu, P.Liu, D. Jiang, L. Ma and W. Shen, Electrochemically induced Ti^{3+} self-doping of TiO_2 nanotube arrays for improved photoelectrochemical water splitting. J. Mater Sci 52 (2017) 6976.

[40] Q. Kang, J. Cao, Y. Zhang, L. Liu, H. Xu and J. Ye, Reduced TiO_2 nanotube arrays for photoelectrochemical water splitting. J. Mater. Chem. A 1 (2013) 5766.

[41] A.G.Muñoz, Semiconducting properties of self-organized TiO_2 nanotubes. Electrochim. Acta 52 (2007) 4167.

[42] D. W. Kim, N. Enomoto, Z. Nakagawa and K. Kawamura, Molecular Dynamic Simulation in Titanium Dioxide Polymorphs: Rutile, Brookite, and Anatase J. Am. Ceram. Soc.,79 (1996) 1095.

[43] H. Gruber and E. Krautz, Magnetoresistance and Conductivity in the Binary System Titanium–Oxygen. I. Titanium Oxides with Metallic Conductivity, Phys. Status Solidi A 69 (1982) 287.

[44] M. Okada, P. Jing, Y. Yamada, M. Tazawa, K. Yoshimura, Low-energy electron energy loss spectroscopy of rutile and anatase TiO 2 films in the core electron excitation regions, Surf. Sci. 566–568 (2004) 1030.

[45] G. Bertoni E. Beyers, J. Verbeeck, M. Mertens, P. Cool, E.F. Vansant, G. Van Tendeloo ,Quantification of crystalline and amorphous content in porous TiO_2 samples from electron energy loss spectroscopy, Ultramicroscopy 106 (2006) 630.

[46] E. Stoyanov, F. Langenhorst, G. Steinle-Neumann, The effect of valence state and site geometry on Ti $L_{3,2}$ and O K electron energy-loss spectra of Ti_xO_y phases, 92 (2007) 577.

[47] C.-N. Huang, J.-S. Bow, Y. Zheng, S.-Y. Chen, N.J. Ho, P. Shen, Nonstoichiometric Titanium Oxides via Pulsed Laser Ablation in Water, Nanoscale Res. Lett. 5 (2010) 972.

Figure captions

Figure 1. (A) SEM cross-sectional image of the annealed TiO_2 nanotube layer grown on the GoFe99.99 Ti substrate; (B) average inner tube diameter and thickness of the TiO_2 nanotube layers grown on all 4 substrates.

Figure 2. (A) Photocurrent densities and (B) IPCE recorded upon illumination of the annealed (400 °C for 1 hour) nanotube layers shown in Fig. 1 by monochromatic light, in the range of wavelengths from 300 to 400 nm (step 5 nm); (C and D) photocurrent density transients recorded for 10 and 1000 s under illumination by monochromatic UV light (λ = 340 nm, intensity of 0.18 mW/cm^2). All values were recorded at 0.4 V vs. Ag/AgCl in 0.1 M Na_2SO_4 and electrolyte.

Figure 3. (A) CV curves recorded for TiO_2 nanotube layers grown on different Ti substrates in the dark (solid lines) and under UV light illumination (λ = 340 nm, dashed lines); (B) Mott–Schottky plots of TiO_2 nanotube layers grown on different Ti substrates collected at a frequency of 1 kHz in the range of voltages from 1 to -0.4 V in the dark.

Figure 4. XRD patterns of the nanotube layers grown on different substrates shows peak positions of A = TiO_2 anatase, Ti = metallic titanium.

Figure 5. (A) HAADF STEM image of a typical area of EELS data collection, (B) EELS Ti: $L_{2,3}$-edge of Ti sheets, (C) EELS Ti: $L_{2,3}$-edge of TiO_2 nanotube layers grown from different substrates and (D) EELS O: K-edge of TiO_2 nanotube layers grown from different substrates.

Figures

Figure 1

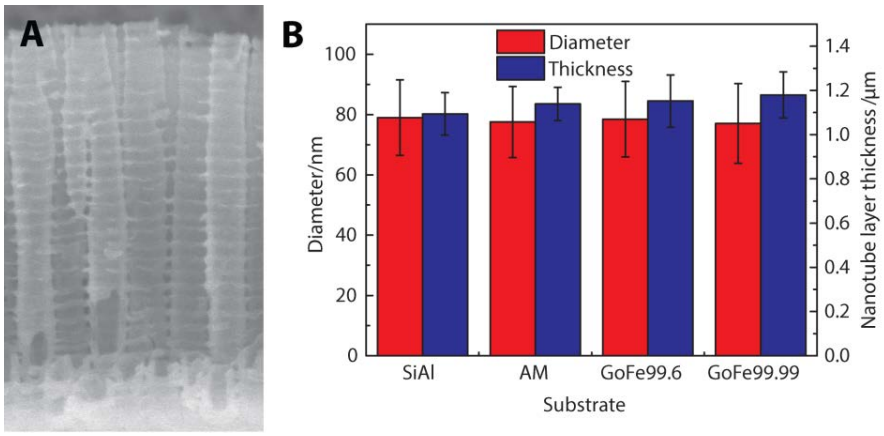

Figure 2

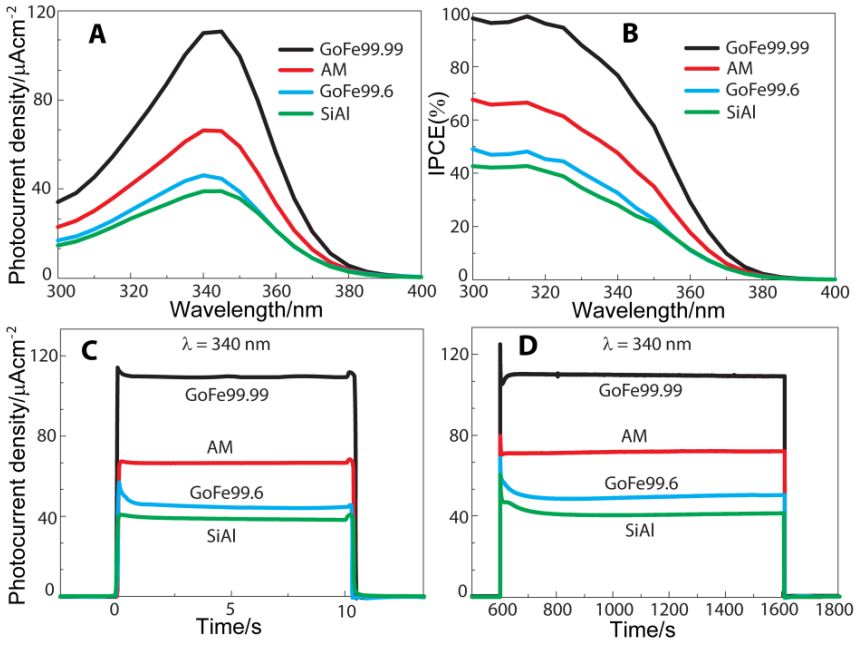

Figure 3

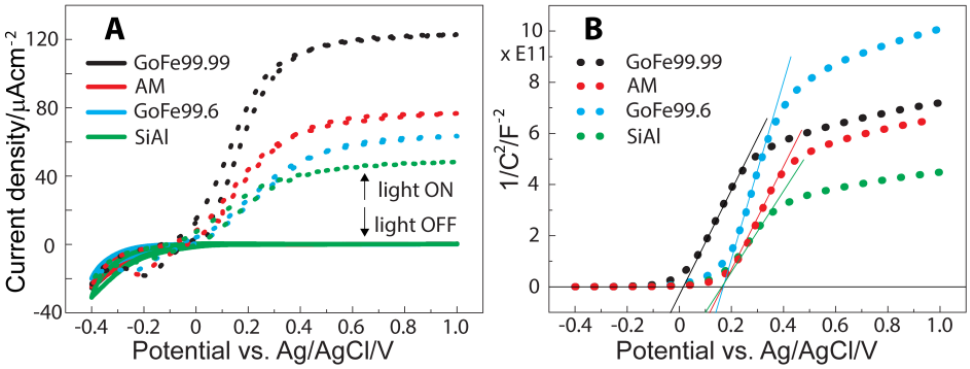

Figure 4

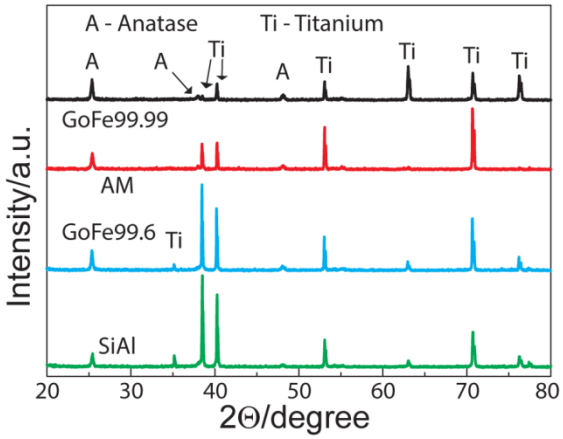

Figure 5